

2

3

Geophysical Research Letters

4

Supporting Information for

5 **Global analysis of surface ocean CO₂ fugacity and air-sea fluxes with low latency**

6

T. T. T. Chau¹, F. Chevallier¹, and M. Gehlen¹

7

¹Laboratoire des Sciences du Climat et de l'Environnement, LSCE/IPSL, CEA-CNRS-UVSQ, Université
8 Paris-Saclay, F-91191 Gif-sur-Yvette, France

9

10

11 **Contents of this file**

12

13 1. Evaluation and analysis for surface ocean CO₂ fugacity and air-sea fluxes

14 2. Tables S1 to S5

15 3. Figures S1 to S10

16 4. References

17

18

19 1. Evaluation and analysis for surface ocean CO₂ fugacity and air-sea fluxes

20 1.1. Quality assessment for regional reconstruction and prediction of CO₂ 21 fugacity ($f\text{CO}_2$)

22 In reconstruction mode (1985-2020), FFNNv2021 and FFNNv2 models perform with
23 good skill over many ocean provinces (Figures 2, S3, and S5). Subtropical and tropical
24 provinces (i.e., 3.NA-PS, 5.SA, 7.NP-PS, 8.PEQU-W, 10.SP, and 12.SIO) have the highest
25 scores (RMSD < 14 μatm and r^2 > 0.74). Interestingly, these sub-basins are not
26 dominant in data density compared to subpolar regions (2.NA-SS and 6.NP-SS) for the
27 northern hemisphere and to the southern ocean (13.SO-SS) for the southern
28 hemisphere (Figure 2). Data-rich provinces involve many observations distributed in
29 coastal bands or in ocean upwelling systems with substantial $f\text{CO}_2$ inter-annual
30 variations. These data put high weight on the calculated model-data mismatch (Figures
31 S5 and S6). The model tends to get high biases from SOCAT data outliers (Figure S3),
32 i.e., data beyond the 95% confidence interval ([279, 443] μatm) of the full data range.
33 Overestimates of $f\text{CO}_2$ with a model-data bias greater than 100 μatm are distributed
34 along the Arctic (1.ARC) and the subpolar-polar regions (2.NA-SS, 6.NP-SS, and
35 14.SO-ICE) (Figure S3 and Figure S5). Most of the poor estimates of $f\text{CO}_2$ belong to the
36 coastal sector of these regions (Figure S5) where $f\text{CO}_2$ is characterized with high
37 variability driven by multiple and complex physical and biological conditions (Feely et
38 al., 2008; Bakker et al., 2016; Chavez et al., 2018; Chau et al., 2022). RMSD ranges from
39 21.1 μatm to 40 μatm and r^2 is between 0.57 and 0.76 over these regimes. In contrast,
40 the FFNN models underestimate SOCAT $f\text{CO}_2$ at the right tail of its global distribution.
41 Most of these data belong to the coastal sectors of NA-SS and NP-SS or are found in
42 PEQU-E and NIO (see further analysis in Chau et al. (2022). Among these provinces, the
43 eastern equatorial Pacific (9.PEQU-E) yields the largest RMSD (~27 μatm). Nevertheless,
44 the reconstruction of the interannual variability of $f\text{CO}_2$ over PEQU-E has an r^2 of 0.71.

45
46 Despite general good performance as analyzed in the main manuscript, FFNNv2021
47 shows the poorest one-year prediction in 2021 relative to the 1985-2020 reconstruction
48 skill in ARC (RMSD: 49.1 μatm vs 40 μatm ; r^2 : 0.25 vs 0.57), in AEQU (RMSD: 34.2 μatm vs
49 19.96 μatm ; r^2 : 0.36 vs 0.57), and in PEQU-E (RMSD: 37.2 μatm vs 27 μatm ; r^2 : 0.55 vs
50 0.71). The FFNNv2022 model reconstruction in 2021 benefits from more than 919
51 additional data (411 data points in the year 2021), resulting in an improvement in the
52 $f\text{CO}_2$ estimates in 2021 over the Arctic: the RMSD reduces to 41.8 μatm and r^2 rises up
53 to 0.35 (Figure S7). In 2022, the FFNNv2022 model scores slightly better in one-year

prediction (RMSD = 37.0 μatm and $r^2 = 0.60$) relative to the FFNNv2021 two-year prediction (RMSD = 37.7 μatm and $r^2 = 0.56$). To a smaller extent, this improvement holds for the equatorial Atlantic (4.AEQU) and the eastern equatorial Pacific (9.PEQU-E). For instance, the FFNNv2021 prediction (RMSD = 34.2 μatm and $r^2 = 0.36$) in AEQU in 2021 shows similar skill scores compared to the FFNNv2022 reconstruction (RMSD = 32.9 μatm and $r^2 = 0.43$). By contrast, the two model predictions perform well in 2022 (RMSD < 17.5 μatm and $r^2 < 0.6$), knowing that the evaluation data in SOCATv2023 in the years 2021 and 2022 do not have the same quantity and distribution over AEQU as well as other ocean provinces (Table S4 and Figure S5). For both reconstruction and prediction modes, the two time series of the mean $f\text{CO}_2$ derived from the two models deviate in interannual variability of $f\text{CO}_2$ in the equatorial Atlantic (Figure S6). Over the equatorial Pacific (9.PEQU-E), FFNNv2022 predicts $f\text{CO}_2$ in 2022 with a high deviation from SOCAT data (RMSD = 47.1 μatm) but reproduces its temporal variations well ($r^2 = 0.76$). FFNNv2021 makes the two-year prediction (RMSD = 45.1 μatm and $r^2 = 0.77$) marginally more precise than the latest model. The contradictory effects observed in the two FFNN performances over the tropical regions (4.AEQU and 9.PEQU-E) may derive from the discrepancy in SOCAT data used for model fits from one to another version; e.g., SOCATv2022 removed 234 [164] data from the previous version over AEQU [PEQU-E] for the period 1985-2020 (7% [2%] of the total data in this region) and added 116 [180] data for the year 2021 (Figures S2 and S7 and Table S4).

1.2. Computation of air-sea fluxes ($f\text{gCO}_2$)

An air-sea flux density of CO_2 is calculated in $\text{molC.m}^{-2}.\text{yr}^{-1}$ by using the formulation as follows,

$$f\text{gCO}_2 = K \times d\text{pCO}_2 = k \times L \times (1 - f_{\text{ice}}) \times (p\text{CO}_2^{\text{air}} - p\text{CO}_2^{\text{sea}}), \quad (1)$$

where K is the gas transfer coefficient and $d\text{pCO}_2$ is the air-sea difference in partial pressure of CO_2 ($p\text{CO}_2$). K is the product of gas transfer velocity (k), temperature-dependent solubility of CO_2 (L), and sea ice coverage ratio (f_{ice}). L is estimated with sea surface temperature (Weiss, 1974) while the computation of k relies on a quadratic dependence of 10-m wind speed (Ho et al., 2006; Wanninkhof, 2014) and a scaling to match the global mean k of 16.5 cm.h^{-1} (Naegler, 2009). The derivation of atmospheric partial pressure of CO_2 ($p\text{CO}_2^{\text{air}}$) comes from CO_2 mole fraction multiplied with total pressure in dry air conditions. $p\text{CO}_2^{\text{sea}}$ is converted from FFNN $f\text{CO}_2$ following Körtzinger, (1999). Data products used in the air-sea flux

calculation are presented in Table S1. Given flux density per grid cell ($fgCO_2^{(i)}$), an integration of CO_2 fluxes ($PgC.yr^{-1}$) over a region or the global ocean derives from

$$fgCO_2 = \sum_{i=1:N} fgCO_2^{(i)} \times A^{(i)}, \quad (2)$$

where $A^{(i)}$ is the area in m^2 of grid cell (i).

1.3. Multi-year time series of fCO_2 and $fgCO_2$

Figures S6 and S8 (right sector of the red vertical line) respectively show the time series of mean fCO_2 predicted with FFNNv2022 models and of $fgCO_2$ integrated over different provinces. fCO_2 predicted for 2022 continues to increase resulting in an increment of the global average of sea surface partial pressure of CO_2 (pCO_2^{sea}) of 2.9 μatm relative to the year 2021 (Table S5) and much higher than its global growth rate of 1.7 $\mu atm.yr^{-1}$ (2.0 $\mu atm.yr^{-1}$) estimated over the period 1985-2022 (2010s). The one-year increment in atmospheric pCO_2 (pCO_2^{air}) between the two years (2.5 μatm) is less than in pCO_2^{sea} implying a reduction in the global ocean uptake of CO_2 predicted for 2022 ($2.25 \pm 0.5 PgC.yr^{-1}$) compared to the previous year ($2.36 \pm 0.43 PgC.yr^{-1}$). When adjusting the estimated global net fluxes with the riverine outgassing of CO_2 of 0.65 $PgC.yr^{-1}$ (Regnier et al., 2022) and the total ocean surface area (FFNNv2022 data covers 95% of the global ocean), one obtains the estimates of anthropogenic ocean carbon uptake about $3.13 \pm 0.46 PgC.yr^{-1}$ and $3.02 \pm 0.52 PgC.yr^{-1}$ in 2021 and 2022, respectively. The non-increasing imprint in the ocean sink of anthropogenic CO_2 found in this study is consistent with the 2022 projection proposed by Friedlingstein et al, (2022): the anthropogenic ocean sink in 2021 was $2.9 \pm 0.4 PgC.yr^{-1}$ remains unchanged for the year 2022. This evidence supports the hypothesis that the persistence of cooling climate patterns (La Niña conditions) weakened CO_2 ocean uptake in 2021-2022 (high peaks appeared in mid-2022, Figure S9). For January to August in 2023, FFNNv2022 predicts a global net flux of $2.45 \pm 0.56 PgC.yr^{-1}$ (w.r.s.t., $3.23 \pm 0.59 PgC.yr^{-1}$ for anthropogenic uptake) higher than the 8-month net flux in 2022 of $2.17 \pm 0.50 PgC.yr^{-1}$ (w.r.s.t., $2.94 \pm 0.53 PgC.yr^{-1}$ for anthropogenic uptake).

1.4. Substantial intra- to inter-annual changes of fCO_2 and air-sea fluxes ($fgCO_2$) at the eastern equatorial Pacific (EEP) driven by the El Niño Southern Oscillation (ENSO)

The ENSO phenomenon does not only constrain ocean CO_2 outgassing at the tropical Pacific air-sea interface but also strongly affects the global net CO_2 uptake (Rödenbeck et al., 2015; Chau et al., 2022; Friedlingstein et al., 2022). In El Niño conditions, warmer

surface temperature weakens vertical upwelling of subsurface water rich in dissolved inorganic carbon (DIC) and nutrients, therefore, El Niño leads to lower surface partial pressure of CO₂ (Feely et al., 2006; Wang et al., 2015). A decrease of $f\text{CO}_2$ reached 410 μatm and the intra-annual variation of $f\text{CO}_2$ was as large as 40 μatm in the year 2015 (Figure S6) as the strongest El Niño events of the last decade happened (Figure S9a). The dampening $f\text{CO}_2$ resulted in a reduction of the EEP source of CO₂ and thus an enhancement in the global ocean CO₂ uptake (Figure S8). The net flux exceeded $-0.15 \pm 0.03 \text{ PgC.yr}^{-1}$ in 2015/2016 while the EEP normally released an average source of CO₂ of $-0.31 \pm 0.02 \text{ PgC.yr}^{-1}$ in the last decade. The spatial pattern in Figure S9bc confirms that the El Niño events spreading until the 2016 summer probably reduced $f\text{CO}_2$ below 400 μatm ($f\text{gCO}_2 < -0.5 \text{ molC.m}^{-2}.\text{yr}^{-1}$) around 90°W and 150°W westward. Later in this period, the opposite conditions - La Niña - triggered in the 2017 summer became dominant and $f\text{CO}_2$ was, for the first time, rising over 460 μatm in the 2018 spring. La Niña has turned back and governed since the year 2020 (Figure S9a). The cooling phase persisted in 2021 and reached its maximum in the 2022 spring-summer. Anomalies in $f\text{CO}_2$ enhancement have been found throughout the year 2021 (Figure S9(b,c)). Likewise, FNNv2022 correspondingly projects extremely high $f\text{CO}_2$ exceeding 484 μatm ($f\text{gCO}_2 < -2.5 \text{ molC.m}^{-2}.\text{yr}^{-1}$) in the eastern Niño3 and Niño4 sectors in the first half of 2022. By then, a reduction of $f\text{CO}_2$ is predicted according to the lessening cooling conditions.

2. Tables

Table S1. Input datasets used for reconstructions and prediction of surface ocean CO₂ fugacity ($f\text{CO}_2$) and air-sea fluxes ($f\text{gCO}_2$) in 1985-2023.

Variables	Notation	Product name	References
Measurements of CO ₂ fugacity	$f\text{CO}_2$	Surface ocean CO2 ATlas (SOCAT): SOCATv2021 , SOCATv2022 (last access 17/06/2022), and SOCATv2023 (last access 20/06/2023)	Bakker et al. (2021, 2022, 2023)
Sea surface temperature	SST	Copernicus Marine Service (CMEMS): SST_GLO_SST_L4_REP_OBSERVATIONS_010_011 (1985-2021)	Good et al. (2020)
Sea ice fraction	f_{ice}	SST_GLO_SST_L4_NRT_OBSERVATIONS_010_001 (2022-2023)	
Sea surface salinity	SSS	CMEMS: MULTIOBS_GLO_PHY_S_SURFACE_MYNRT_015_013 (1993-2023)	Buongiorno et al. (2016); Droghei et al. (2018)
Sea surface height	SSH	CMEMS: SEALEVEL_GLO_PHY_L4_MY_008_047 (1993-2021) SEALEVEL_GLO_PHY_L4_NRT_OBSERVATIONS_008_046 (2022-2023)	Pujol et al. (2016, 2018)

Mixed layer depth	MLD	Estimating the Circulation and Climate of the Ocean project Phase II (ECCO2): cube92_latlon_quart_90S90N (1992-2022)	Menemenlis et al. (2008)
Chlorophyll- <i>a</i>	Chl- <i>a</i>	CMEMS: OCEANCOLOUR GLO BGC L4 MY 009 104 (1998-2023)	Garnesson et al. (2019)
Atmospheric CO ₂ mole fraction	xCO ₂	CO ₂ atmospheric inversion from the Copernicus Atmosphere Monitoring Service (CAMS): Surface: v20r2 (1985-2020) Satellite: FT21r2 (2021)	Chevallier et al. (2005, 2010); Chevallier. (2013)
pCO ₂ climatology	pCO ₂ ^{cli} _m	Lamont Doherty Earth Observatory (LDEO) climatology of sea surface partial pressure of CO ₂	Takahashi et al. (2009)
Wind speed	U	ERA5 hourly data on single levels from 1959 to present (1985-2023)	Hersbach et al., (2020)
Total pressure	P _s		

143 Notes:

- 144 • Preprocessing for missing data in the reconstruction mode (before the 2000s):
 - 145 ○ SSS and CHL-*a* (MLD) are set to climatologies computed on the available
 - 146 data (in 1992-1997).
 - 147 ○ SSH is set to climatologies plus linear trends computed on the available
 - 148 data
- 149 • Preprocessing for missing data in the prediction mode (2022-2023):

150 Input datasets for prediction are set to the same data resources as for
 151 reconstruction, these data are available within a few weeks behind real
 152 time. This condition is not met for the xCO₂ and MLD datasets that we
 153 use in 2023. For xCO₂, we extrapolated the original dataset (the
 154 atmospheric inversion of the Copernicus Atmosphere Monitoring Service
 155 for years 1985- 2022, Table S1), knowing the recent measurements of the
 156 atmospheric CO₂ mole fraction at the Mauna Loa Observatory, Hawaii
 157 (<https://gml.noaa.gov/ccgg/trends/mlo.html>, last access: 11/9/2023). For
 158 MLD, given the dominance of seasonality in its variability (Menemenlis et
 159 al. 2008, Zhang et al. 2018), we use the last 5-year climatology of the
 160 Estimating the Circulation and Climate of the Ocean project Phase II
 161 (ECCO2) data in the prediction mode.

162 **Table S2. Indicators of ocean provinces (Figure S1) used in this study.**

No	Ocean provinces	Remarks
0	Global ocean (GLO)	

1	Arctic (ARC)	Aggregated from Arctic, North Atlantic, and North Pacific ice biomes and the Barents Sea (biomes 1, 2, 3, and 4)
2	North Atlantic seasonally stratified (NA-SS)	Aggregated from North Atlantic subpolar and subtropical seasonally stratified biomes (biomes 5 and 6)
3	North Atlantic permanently stratified (NA-PS)	North Atlantic subtropical permanently stratified biome (biome 7)
4	Atlantic equatorial (AEQU)	Biome 8
5	South Atlantic (SA)	South Atlantic subtropical permanently stratified biome (biome 9)
6	North Pacific seasonally stratified (NP-SS)	Aggregated from North Pacific subpolar and subtropical seasonally stratified biomes (biomes 11 and 12)
7	North Pacific permanently stratified (NP-PS)	North Pacific subtropical permanently stratified biome (biome 13)
8	Pacific western equatorial (PEQU-W)	Biome 14
9	Pacific eastern equatorial (PEQU-E)	Biome 15
10	South Pacific (SP)	South Pacific subtropical permanently stratified biome (Biome 16)
11	Northern Indian Ocean (NIO)	Aggregated from the Arabian Sea, Bay of Bengal, and Equatorial Indian Ocean above the Equator (biomes 17, 18, and 19)
12	Southern Indian Ocean (SIO)	Aggregated from the Equatorial Indian Ocean below the Equator and the South Indian Ocean (biomes 19 and 20)
13	Southern Ocean seasonally stratified (SO-SS)	Aggregated from Southern Ocean subpolar and subtropical seasonally stratified biomes (biomes 21 and 22)
14	Southern Ocean icea (SO-ICE)	Biome 23

163

164 **Table S3. Comparison of CMEMS-LSCE-FFNN models (FFNNv2021 and FFNNv2022)**

165 **a) Summary of SOCAT data used for model runs and model evaluation**

FFNN	Model fitting			Model evaluation				
	Target Data	Time span	Number of data	Target Data	Reconstruction		Prediction	
					Time span	Number of data	Time span	Number of data

v2021	SOCATv2021	1985-2020	306357	SOCATv2023	1985-2020	302255	2021-2022	109088602
v2022	SOCATv2022	1985-2021	311694		1985-2021	313163	2022	8602

166

167

168

169

170

171

b) Model evaluation between global reconstructions of $f\text{CO}_2$ [μatm] in 1985-2020 and between FFNNv2021 prediction and FFNNv2022 reconstruction (prediction) in 2021 (2022). Statistics include the number of SOCAT monthly gridded data (N), mean $f\text{CO}_2$ (μ), mean uncertainty (σ), and model-data misfit (RMSD) and coefficient of determination (r^2).

FFNN	Years											
	1985-2020				2021				2022			
	μ	σ	RMSD	r^2	μ	σ	RMSD	r^2	μ	σ	RMSD	r^2
v2021	361.6	8.7	19.1	0.78	395.2	11.4	24.3	0.74	397.8	12.2	23.1	0.75
v2022	361.5	8.5	19.1	0.78	395.7	10.9	23.3	0.76	398.5	11.3	22.6	0.76

172

Table S4. Regional comparison (a) between FFNN model reconstructions of $f\text{CO}_2$ [μatm] in 1985-2020, (b) between FFNNv2021 prediction and FFNNv2022 reconstruction in 2021, and (c) between FFNN model predictions in 2022. Statistics include 1) the number (N) of monthly gridded data used in FFNN fits (SOCATv2021 and SOCATv2022) and in data evaluation (SOCATv2023, see values in brackets), 2) mean $f\text{CO}_2$ (μ), 3) mean uncertainty (σ), and 4) model-data misfit (RMSD), and 5) determination coefficient (r^2).

No	Biome	FFNN	Years														
			1985-2020					2021					2022				
			N	μ	σ	RMSD	r^2	N	μ	σ	RMSD	r^2	N	μ	σ	RMSD	r^2
1	ARC	v2021	5043 (5646)	320.5	30.0	40.0	0.57	0 (411)	356.3	31.3	49.1	0.25	0 (225)	351.4	29.6	37.7	0.56
		v2022	5551	318.0	29.3	40.0	0.57	411	348.5	29.5	41.8	0.35	0	345.	27.5	37.0	0.60
2	NA-SS	v2021	57808 (55738)	339.8	8.0	23.1	0.76	0 (2350)	368.8	9.0	26.0	0.76	0 (2265)	373.6	10.1	24.6	0.74
		v2022	55714	339.9	7.7	23.1	0.76	2167	369.1	8.3	26.2	0.75	0	374.	9.1	24.0	0.75

			(5646)					(411)					(225)	6			
			(55738)					(2350)					(2265)	8			
3	NA-PS	v2021	37951 (37011)	364.5	5.3	13.9	0.74	0 (1161)	398.4	6.3	20.4	0.50	0 (1007)	401.0	7.0	18.2	0.61
		v2022	36991 (37011)	364.5	5.1	13.8	0.75	945 (1161)	399.3	5.9	20.1	0.51	0 (1007)	402.7	6.5	17.0	0.65
4	AEQU	v2021	3313 (3179)	376.9	10.0	20.0	0.57	0 (182)	400.2	12.8	34.2	0.36	0 (144)	403.1	14.2	17.3	0.64
		v2022	3179 (3179)	376.0	10.0	19.9	0.57	116 (182)	400.5	13.2	32.9	0.43	0 (144)	404.2	13.6	16.7	0.65
5	SA	v2021	6575 (6497)	369.6	7.9	13.2	0.79	0 (273)	398.5	9.5	14.3	0.55	0 (161)	401.1	10.2	12.8	0.51
		v2022	6497 (6497)	369.7	7.6	12.9	0.80	212 (273)	401.9	9.2	12.4	0.59	0 (161)	404.3	9.6	12.0	0.55
6	NP-SS	v2021	57531 (58165)	349.1	8.2	21.1	0.73	0 (2334)	378.9	10.1	28.3	0.76	0 (1495)	383.1	11.1	31.0	0.62
		v2022	58161 (58165)	349.5	8.0	21.0	0.74	2147 (2334)	380.8	9.4	27.4	0.77	0 (1495)	385.9	10.2	30.2	0.64
7	NP-PS	v2021	40176 (40300)	360.7	5.3	11.9	0.85	0 (1705)	397.0	7.1	16.4	0.76	0 (1608)	401.3	8.4	13.2	0.78
		v2022	40287 (40300)	360.6	5.1	11.8	0.85	1443 (1705)	397.1	6.5	16.1	0.77	0 (1608)	401.5	7.3	12.4	0.81
8	PEQU-W	v2021	14845 (14821)	366.6	6.1	11.2	0.72	0 (484)	407.2	9.2	11.2	0.76	0 (326)	411.6	10.7	12.0	0.73
		v2022	14821 (14821)	366.6	6.0	11.2	0.72	430 (484)	407.8	8.2	11.1	0.74	0 (326)	411.8	9.1	10.9	0.78
9	PEQU-E	v2021	9470 (9306)	415.7	9.9	27.0	0.71	0 (199)	460.0	14.4	37.2	0.55	0 (146)	462.4	15.7	45.0	0.77
		v2022	9306 (9306)	415.5	9.7	26.9	0.71	180 (199)	459.8 9	13.1	35.2	0.59	0 (146)	461.9	13.8	47.1	0.76
10	SP	v2021	21551 (20968)	363.1	9.0	11.9	0.86	0 (689)	398.4	11.9	10.2	0.85	0 (592)	399.8	12.6	10.1	0.80
		v2022	20968 (20968)	363.5	8.8	11.8	0.87	605 (689)	399.3	11.3	9.8	0.86	0 (592)	400.5	11.5	10.0	0.80
11	NIO	v2021	1335 (1335)	382.8	15.0	24.0	0.53	0 (0)	418.3	23.6	nan	nan	0 (0)	419.8	24.4	nan	nan
		v2022	1335 (1335)	382.1	14.7	23.9	0.54	0 (0)	416.8	23.7	nan	nan	0 (0)	419.7	23.4	nan	nan
12	SIO	v2021	4583 (4562)	357.2	9.3	10.8	0.88	0 (133)	392.6	14.1	11.2	0.80	0 (73)	394.1	14.8	8.8	0.43
		v2022	4562 (4562)	356.7	9.0	10.8	0.88	133 (133)	392.8	13.8	12.0	0.81	0 (73)	394.2	13.6	9.3	0.45

13	SO-SS	v2021	32819 (31424)	351.8	8.4	15.2	0.68	0 (777)	384.4	11.1	15.2	0.66	0 (400)	386. 6	11.7	18.1	0.42
		v2022	31404 (31424)	351.6	8.6	15.1	0.69	624 (777)	384.7	10.6	15.2	0.67	0 (400)	386. 9	11.2	17.9	0.44
14	SO-ICE	v2021	12266 (12277)	362.5	10.7	28.7	0.58	0 (193)	388.6	13.4	24.4	0.44	0 (142)	388. 2	13.5	41.8	0.76
		v2022	12277 (12277)	362.9	10.6	28.6	0.59	185 (193)	388.7	12.7	22.2	0.47	0 (142)	388. 2	13.0	40.9	0.78

180

181 **Table S5. Area-integrated air-sea CO₂ fluxes (*fg*CO₂) derived from FFNNv2022 *f*CO₂**
182 **reconstruction in 1985-2021 and from FFNNv2022 predictions in 2022-2023. The**
183 **units of *fg*CO₂ are in PgC.yr⁻¹. Area-averaged surface temperature (SST), 10-m wind**
184 **speed (U), sea surface partial pressure of CO₂ (*p*CO₂^{sea}), air-sea *p*CO₂ difference**
185 **(*dp*CO₂), and gas transfer coefficient (K) are provided for the global ocean and**
186 **each ocean province (see province indicator in Figure S1).**

187

No	Biome	Area [10 ⁶ km ²]	Years	Variables					
				SST [°C]	U [ms ⁻¹]	<i>p</i> CO ₂ ^{sea} [µatm]	<i>dp</i> CO ₂ [µatm]	K [molC.m ⁻² .y r ⁻¹ .µatm ⁻¹]	<i>fg</i> CO ₂ [PgC.yr ⁻¹]
0	GLO	343.3	1985-2020	18.8	7.8	362.8±10.5	2.8	0.0526	1.583±0.341
			2021	19.0	7.9	397.1±13.0	6.0	0.0524	2.355±0.434
			2022	19.2	7.9	400.0±13.0	5.7	0.0528	2.249±0.495
			2023/01-08	19.1	7.8	401.5±14.1	7.0	0.0519	2.449±0.557
1	ARC	6.9	1985-2020	-0.5	7.3	324.9±33.3	50.3	0.0228	0.082±0.017
			2021	-0.1	7.5	355.5±34.2	55.9	0.026	0.107±0.020
			2022	-0.1	7.5	356.4±32.6	60.0	0.0281	0.106±0.017
			2023/01-08	-0.5	6.5	366.0±39.9	53.8	0.0137	0.077±0.015
2	NA-SS	15.9	1985-2020	11.8	9.2	341.2±9.5	30.4	0.0733	0.384±0.041
			2021	12.3	9.4	370.4±9.8	38.6	0.0750	0.503±0.045
			2022	12.5	9.3	376.1±10.4	37.0	0.0731	0.475±0.048
			2023/01-08	12.0	9.0	376.2±11.2	39.4	0.0697	0.467±0.052

3	NA-PS	22.2	1985-2020	25.1	7.0	365.7±5.9	0.8	0.0397	0.042±0.025
			2021	25.4	7.0	400.6±6.6	3.1	0.0389	0.064±0.027
			2022	25.4	6.9	403.6±7.0	3.5	0.0383	0.073±0.031
			2023/01-08	25.4	6.8	404.2±7.7	5.8	0.037	0.092±0.034
4	AEQU	8.5	1985-2020	26.9	5.5	377.2±12.5	-14.2	0.0254	-0.040±0.010
			2021	27.4	5.5	401.8±15.5	-1.9	0.0251	-0.009±0.017
			2022	27.2	5.5	405.9±15.5	-3.5	0.0245	-0.012±0.016
			2023/01-08	27.6	5.4	404.0±17.1	0.6	0.0241	-0.002±0.018
5	SA	19.5	1985-2020	22.6	7.2	371.0±8.5	-5.2	0.0419	-0.012±0.033
			2021	22.8	7.3	403.2±10.1	0.5	0.0423	0.049±0.048
			2022	22.8	7.2	405.6±10.6	-0.4	0.0406	0.036±0.047
			2023/01-08	23.5	7.1	411.0±11.8	-2.9	0.0405	0.024±0.059
6	NP-SS	24.7	1985-2020	12.7	8.7	350.8±10.2	21.4	0.0651	0.393±0.056
			2021	13.3	8.5	382.2±11.8	27.6	0.0618	0.476±0.060
			2022	13.6	8.6	387.6±12.0	26.4	0.0632	0.477±0.073
			2023/01-08	12.6	8.3	389.1±13.0	27.8	0.0589	0.436±0.078
7	NP-PS	40.2	1985-2020	26.3	7.0	361.7±6.1	2.9	0.0404	0.130±0.040
			2021	26.4	6.9	398.4±7.6	3.7	0.0388	0.152±0.053
			2022	26.5	6.8	402.8±8.2	2.5	0.0373	0.126±0.052
			2023/01-08	26.1	7.1	403.4±8.6	5.1	0.0412	0.176±0.069
8	PEQU-W	13.1	1985-2020	29.3	5.1	367.7±7.6	-7.9	0.0220	-0.023±0.010
			2021	29.4	5.2	409.0±9.4	-12.4	0.0222	-0.040±0.013
			2022	29.3	5.4	413.3±10.0	-14.0	0.0236	-0.052±0.016
			2023/01-08	29.5	5.2	412.1±10.7	-10.2	0.0227	-0.036±0.016
9	PEQU-E	15.1	1985-2020	26.3	5.9	416.8±10.8	-54.0	0.0292	-0.294±0.023
			2021	25.9	6.3	461.3±14.2	-60.8	0.0314	-0.350±0.030
			2022	25.6	6.4	463.5±15.0	-60.4	0.0328	-0.370±0.037

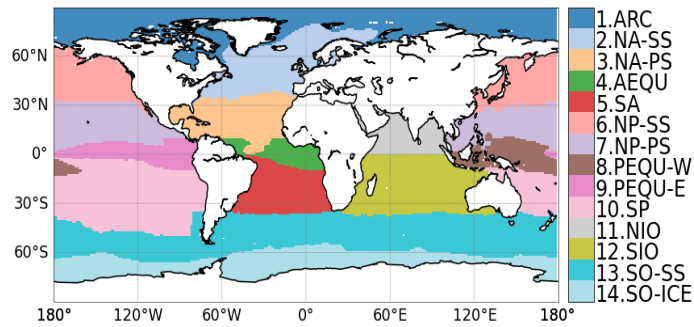
			2023/01-08	27.5	5.8	460.2±15.0	-55.7	0.0277	-0.297±0.036
10	SP	54.8	1985-2020	22.0	7.5	364.7±9.9	0.1	0.0470	0.103±0.117
			2021	22.1	7.6	400.6±12.4	2.6	0.0468	0.161±0.146
			2022	22.0	7.6	401.9±12.5	3.3	0.0464	0.166±0.146
			2023/01-08	22.8	7.5	405.0±13.3	2.2	0.0463	0.201±0.168
11	NIO	11.4	1985-2020	28.2	6.0	383.3±17.0	-21.7	0.0317	-0.113±0.042
			2021	28.5	6.0	418.1±25.8	-19.8	0.0305	-0.099±0.077
			2022	28.4	6.0	421.1±25.2	-20.1	0.0311	-0.104±0.075
			2023/01-08	28.6	6.0	421.3±23.8	-17.4	0.0324	-0.096±0.076
12	SIO	32.9	1985-2020	24.8	7.1	357.8±9.6	5.8	0.0421	0.187±0.064
			2021	25.0	7.2	394.0±14.8	7.1	0.0422	0.216±0.114
			2022	24.9	7.2	395.4±14.5	7.6	0.0423	0.223±0.119
			2023/01-08	25.3	7.1	397.9±13.8	8.1	0.0414	0.222±0.109
13	SO-SS	59.6	1985-2020	8.0	10.5	353.0±9.4	13.3	0.0951	0.721±0.185
			2021	8.2	10.7	386.2±11.6	18.0	0.0956	1.006±0.232
			2022	8.2	10.7	388.4±12.1	17.8	0.0955	0.980±0.269
			2023/01-08	8.7	10.6	391.7±13.4	17.8	0.0950	1.006±0.314
14	SO-ICE	17.3	1985-2020	-1.1	9.1	366.1±11.9	-5.0	0.0421	0.022±0.040
			2021	-1.0	9.1	392.3±14.0	5.2	0.0423	0.119±0.042
			2022	-1.0	9.5	394.4±14.6	4.7	0.0525	0.122±0.054
			2023/01-08	-0.7	9.4	392.3±14.7	11.1	0.0575	0.175±0.073

188

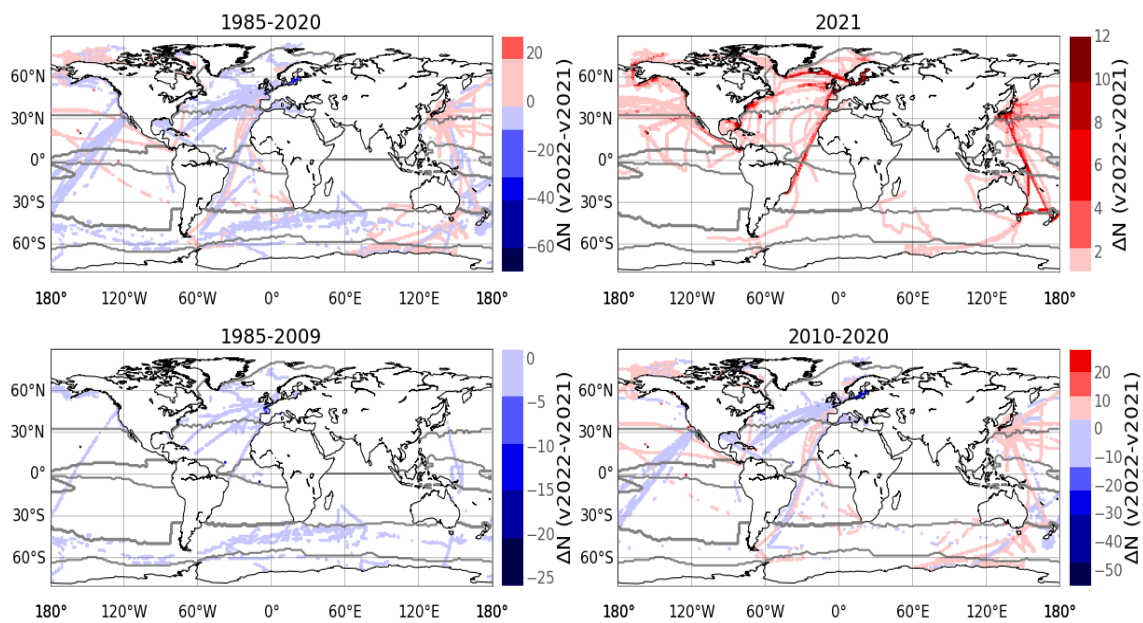
189

190 3. Figures

191



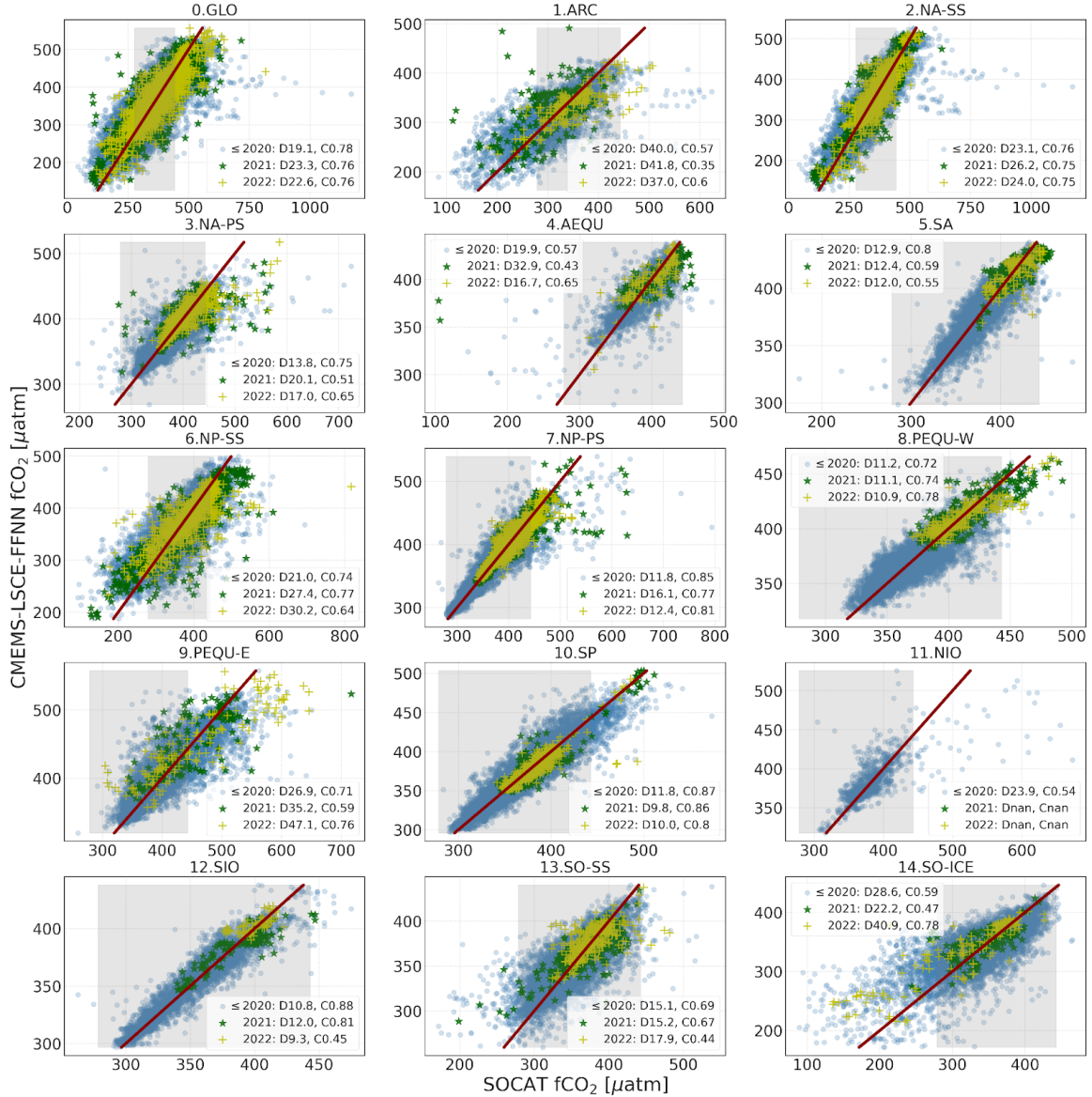
192 **Figure S1.** Ocean provinces aggregated from the biomes used in the RECCAP2
 193 project (source:
 194 <https://github.com/RECCAP2-ocean/RECCAP2-shared-resources/tree/master/data>
 195 /regions, last access: 20/3/2023). See Table S2 for the province indicator.



196

197 **Figure S2.** Number of fCO₂ data (ΔN) added in (red) or removed from (blue)
 198 SOCATv2022 compared to SOCATv2021 for different time frames.

199



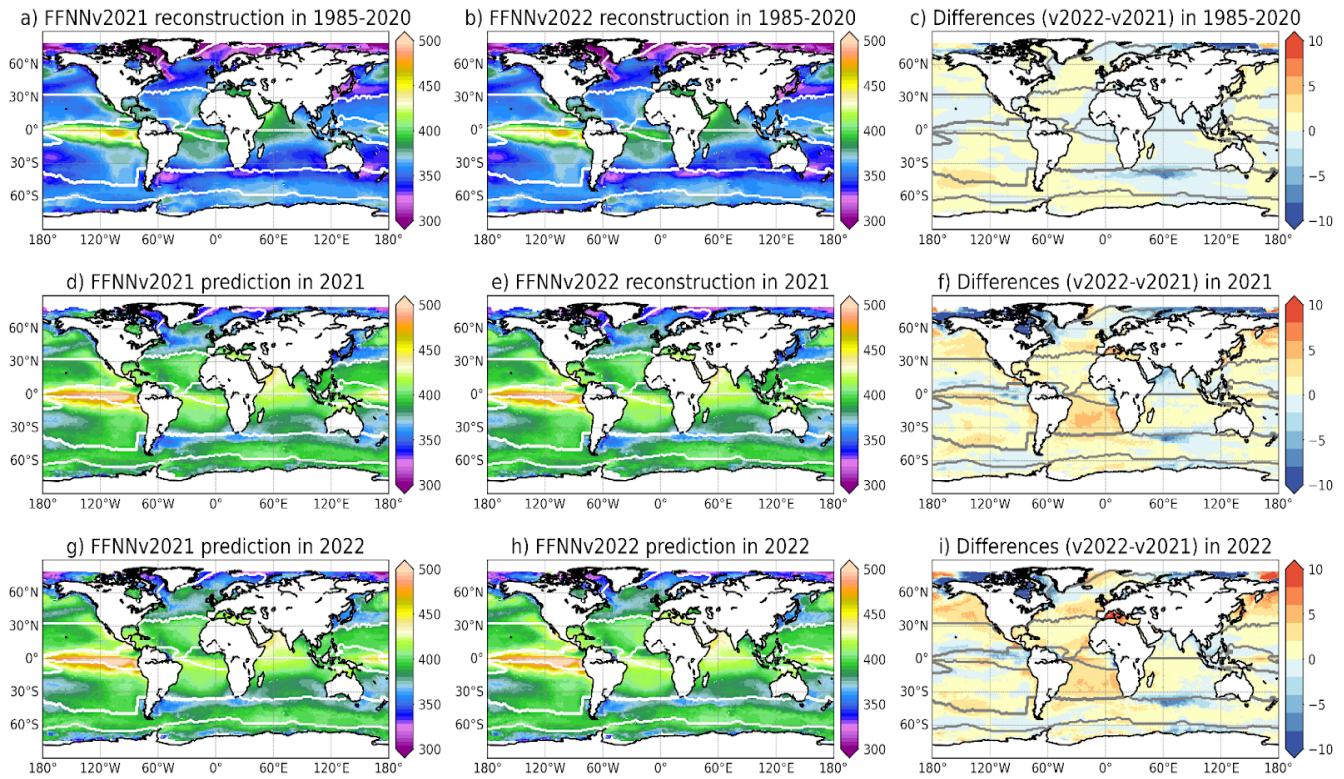
200

201 **Figure S3.** Scatter plots of FFNNv2022 versus SOCATv2023 $f\text{CO}_2$ [μatm] for 36-year
 202 reconstruction (1985-2020: points), 1-year reconstruction (2021: stars) and 1-year
 203 prediction (2022: pluses). Values of FFNNv2022 and SOCATv2023 data are shown
 204 in y- and x-axis, respectively. Light-grey rectangles mark the 95% SOCAT data
 205 range (i.e., [279, 443] μatm) over the global ocean in 1985-2021. Red lines
 206 represent the bisector corresponding to ideal model-data fits: objects above this
 207 line indicate FFNN overestimates of SOCAT $f\text{CO}_2$ and vice versa. Metrics for
 208 reconstruction and prediction in the legend are model-data standard deviation
 209 (D: RMSD) and correlation (C: r^2).

210

211

212



214 **Figure S4.** Spatial distribution of temporal means of $f\text{CO}_2$ derived from FFNNv2021
 215 (left) and FFNNv2022 (middle) and their discrepancy (right).
 216

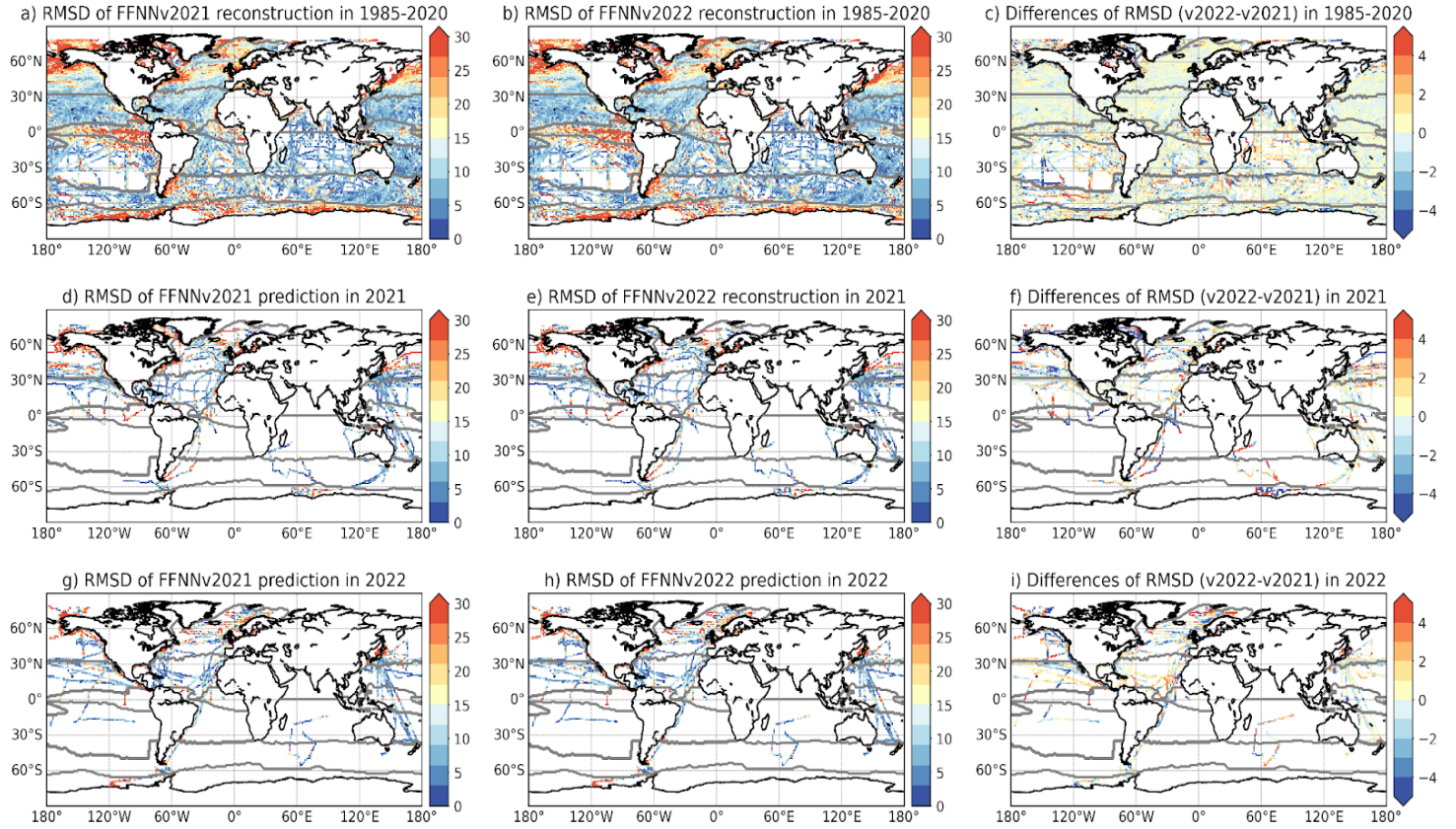


Figure S5. Spatial distribution of model-data deviation (RMSD): $f\text{CO}_2$ derived from FFNNv2021 (left) and FFNNv2022 (middle) and their RMSD difference (right). SOCATv2023 is used for this evaluation.

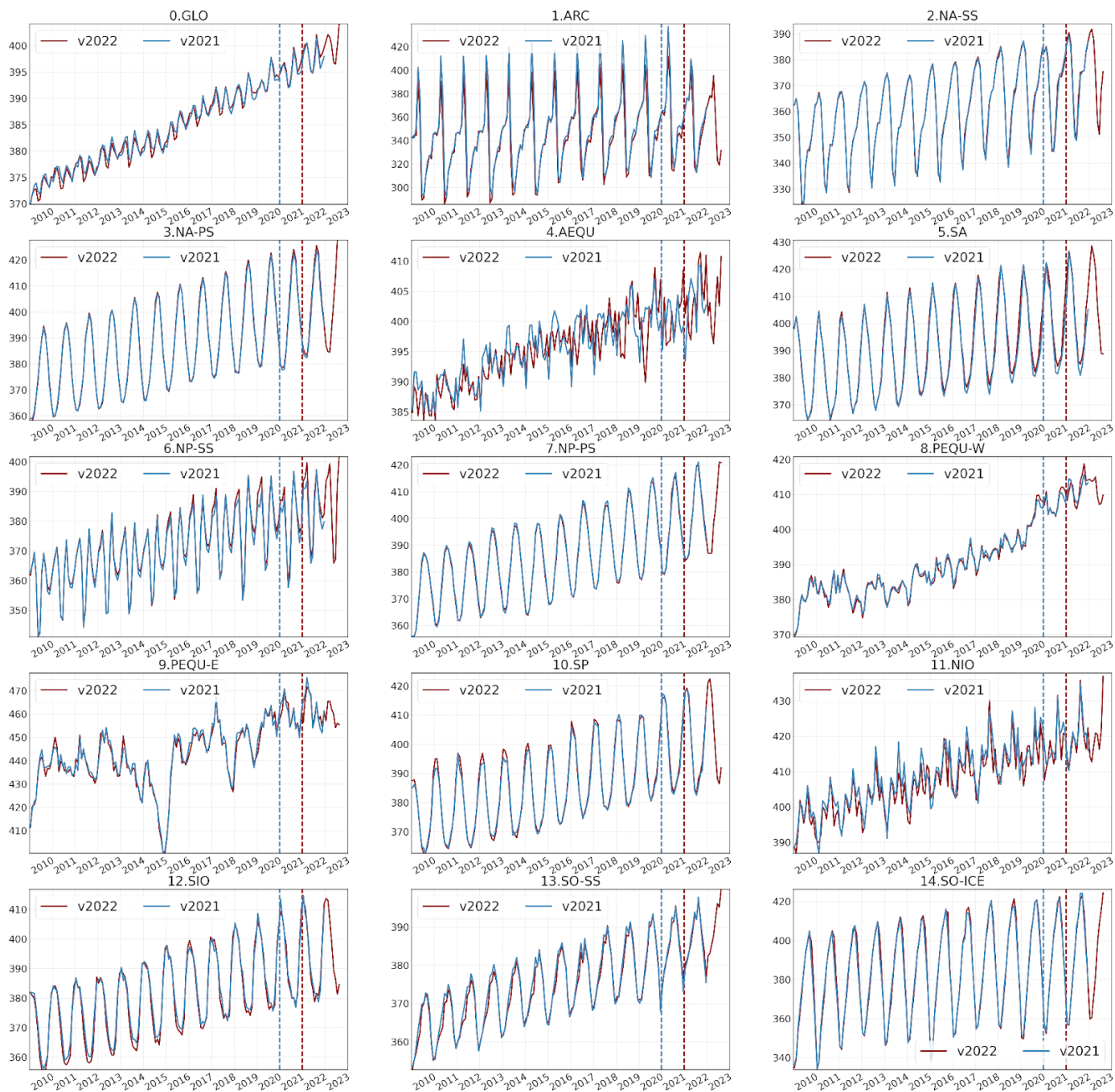
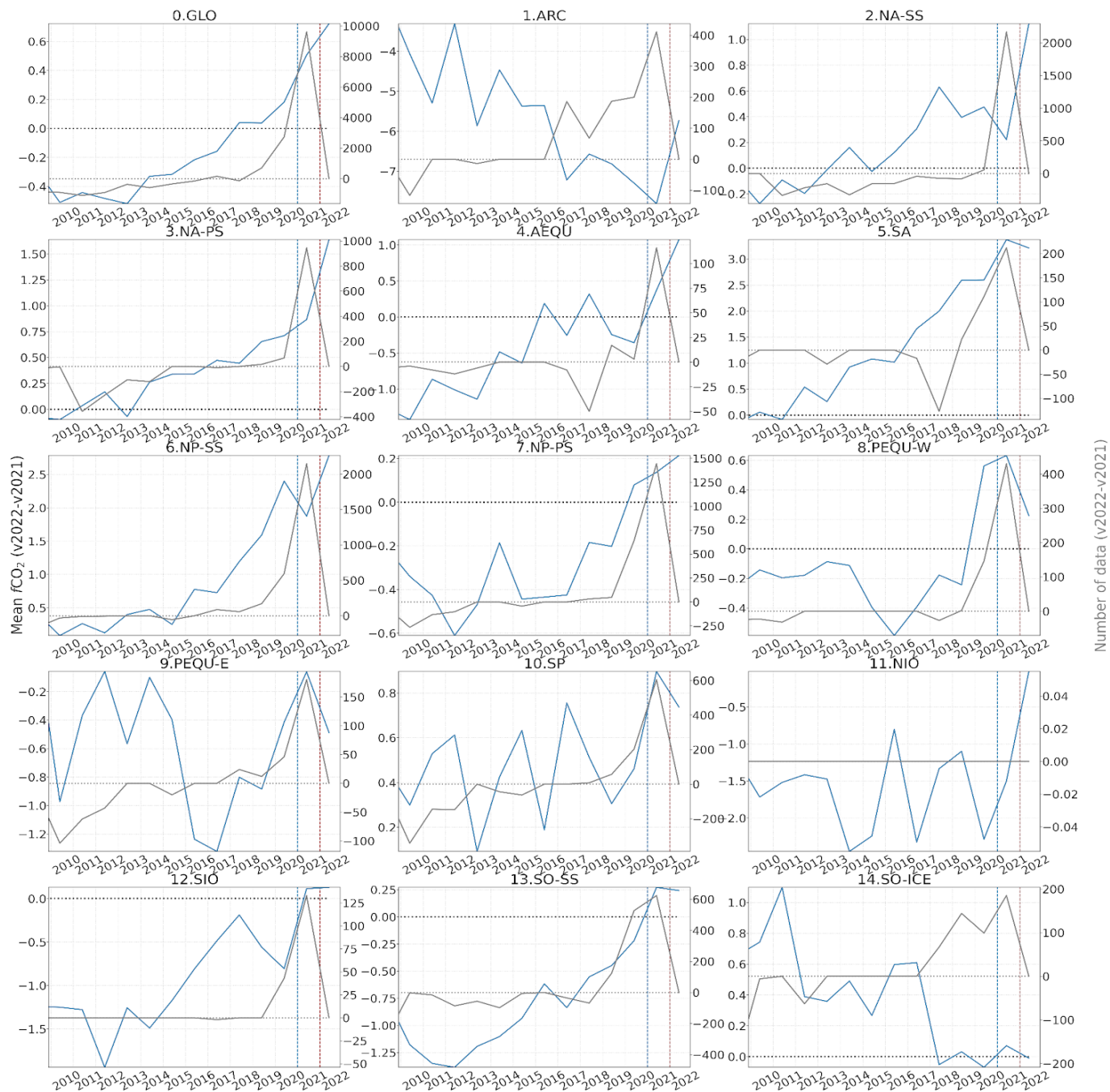


Figure S6. Time series of $f\text{CO}_2$ averaged over ocean provinces. Vertical dashed lines mark the starting date for model prediction (blue: FFNNv2021, red: FFNNv2022).

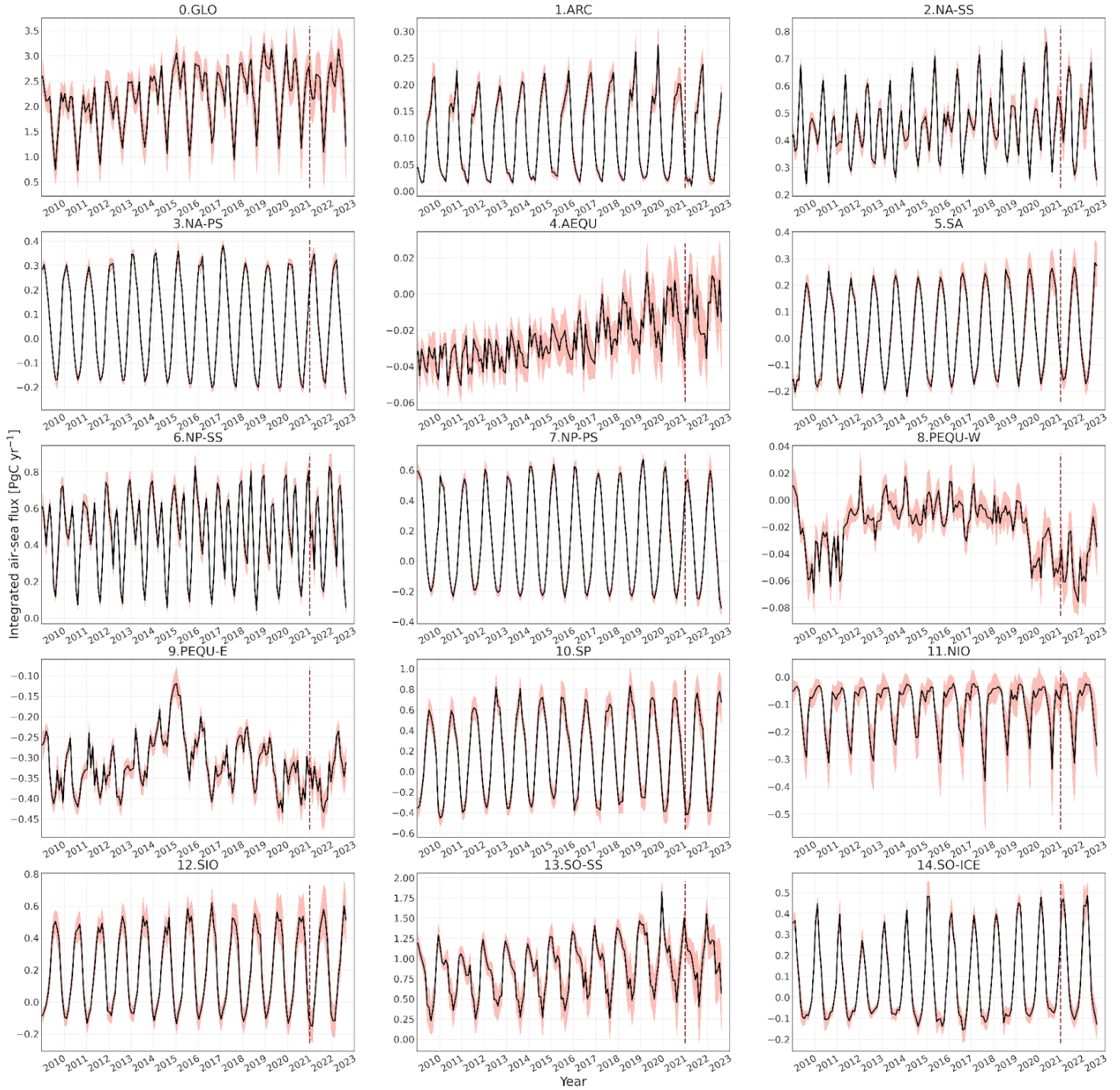


230

231 **Figure S7.** Time series of differences in $f\text{CO}_2$ (left y-axis) and number of SOCAT
 232 data (right y-axis). Vertical dashed line marks the starting date for prediction
 233 (FFNNv2021: blue, FFNNv2022: red).

234

235



237 **Figure S8. Time series of monthly air-sea fluxes integrated over ocean provinces**
 238 **[PgC.yr⁻¹]. Plain curve and shaded area represent model's best estimate and**
 239 **1 σ -uncertainty. Vertical dashed lines mark the starting date for FFNNv2022**
 240 **prediction.**
 241

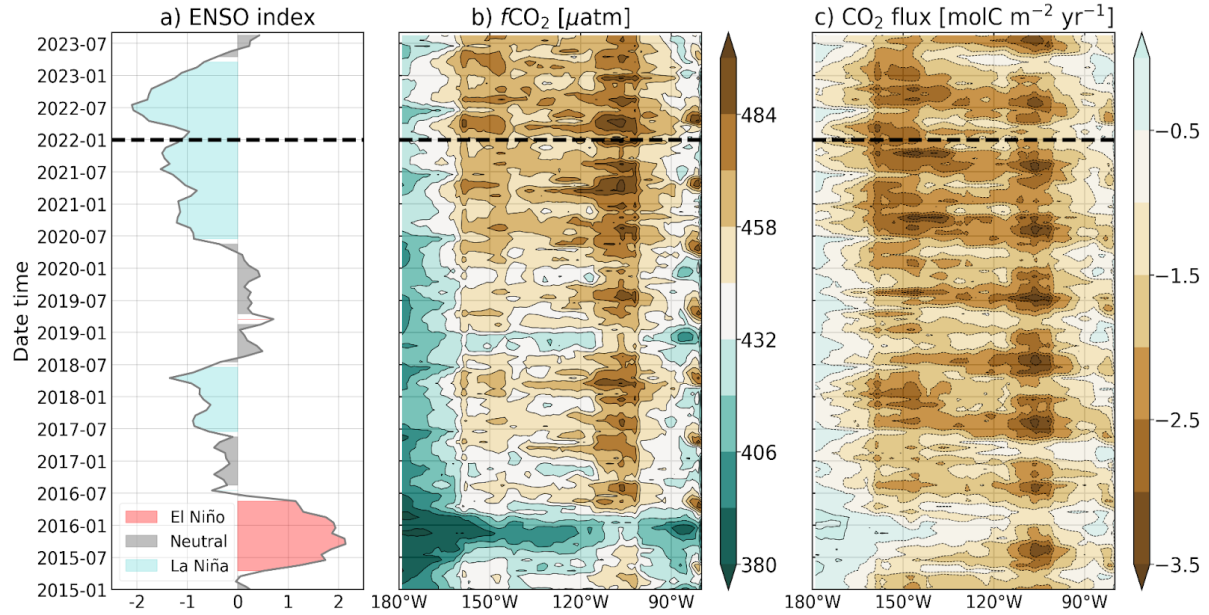


Figure S9. Illustration of the relationship between ENSO events (a) and FFNNv2022 $f\text{CO}_2$ (air-sea fluxes) variations (Hovmöller plots in b and c) over the eastern Equatorial Pacific (9°E-9°W). ENSO events are plotted with the NOAA bi-monthly Multivariate El Niño/Southern Oscillation (ENSO) index (<https://psl.noaa.gov/ens/mei/>, last access: 11/09/2023). The black horizontal dotted line marks the starting date for the FFNNv2022 prediction (January 2022).

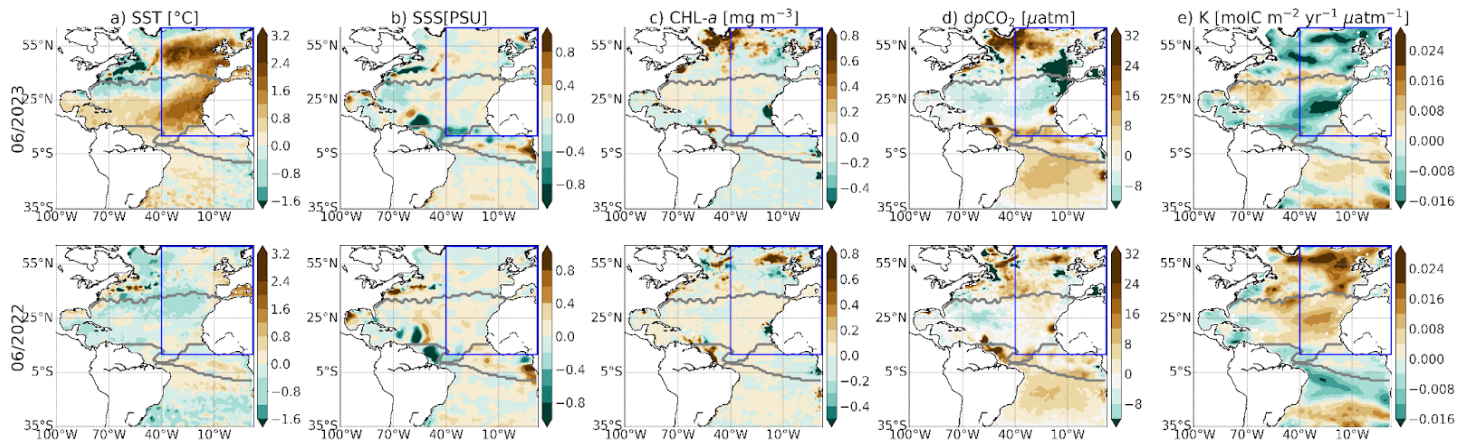


Figure S10. Anomalies of surface temperature (SST), salinity (SSS), Chlorophyll-*a* (CHL-*a*), air-sea $p\text{CO}_2$ difference ($dp\text{CO}_2$), gas transfer coefficient (K) over the Atlantic in June 2023 (top) and June 2022 (bottom) are computed by subtracting long-term trends and seasonal climatologies relative to the years 1985-2022. Blue box limits the region of interest where the extreme marine heat wave appeared in the northeastern Atlantic in June 2023.

259 References

- 260 Bakker, D., Alin, S., Becker, M., Bittig, H., Castaño-Primo, R., Feely, R. A., Gritzalis, T., Kadono, K.,
261 Kozyr, A., Lauvset, S. K., Metzl, N., Munro, D., Nakaoka, S.-i., Nojiri, Y., O'Brien, K., Olsen, A., Pfeil,
262 B., Pierrot, D., Steinhoff, T., Sullivan, K., Sutton, A., Sweeney, C., Tilbrook, B., Wada13, C.,
263 Wanninkhof, R., Wranne, A. W., et al.: SOCAT version 2021 for quantification of ocean CO₂
264 uptake,
265 https://www.socat.info/wp-content/uploads/2022/06/2022_Poster_SOCATv2021_release.pdf,
266 2021.
267
- 268 Bakker, D., Alin, S., Becker, M., Bittig, H., Castaño-Primo, R., Feely, R. A., Gritzalis, T., Kadono, K.,
269 Kozyr, A., Lauvset, S. K., Metzl, N., Munro, D., Nakaoka, S.-i., Nojiri, Y., O'Brien, K., Olsen, A., Pfeil,
270 B., Pierrot, D., Steinhoff, T., Sullivan, K., Sutton, A., Sweeney, C., Tilbrook, B., Wada13, C.,
271 Wanninkhof, R., Wranne, A. W., et al.: SOCAT version 2022 for quantification of ocean CO₂
272 uptake,
273 https://www.socat.info/wp-content/uploads/2022/06/2022_Poster_SOCATv2022_release.pdf,
274 2022.
- 275 Bakker, D., Alin, S. R., Bates, N., Becker, M., Feely, R. A., Gkritzalis, T., . . . others. Surface ocean
276 co₂ atlas database version 2023 (socatv2023). doi: <https://doi.org/10.25921/r7xa-bt92>, 2023.
- 277 Buongiorno Nardelli, B., R. Droghei, and R. Santoleri. Multi-dimensional interpolation of SMOS
278 sea surface salinity with surface temperature and in situ salinity data, *Remote Sens. Environ.*,
279 180, 392–402, doi:10.1016/j.rse.2015.12.052, 2016.
- 280 Chau, T. T. T., Gehlen, M., and Chevallier, F.: A seamless ensemble-based reconstruction of
281 surface ocean *p*CO₂ and air-sea CO₂ fluxes over the global coastal and open oceans,
282 *Biogeosciences*, 19, 1087–1109, <https://doi.org/10.5194/bg-19-1087-2022>, 2022.
- 283 Chavez, F. P., Sevadjan, J., Wahl, C., Friederich, J., & Friederich, G. E. (2018). Measurements of
284 pco₂ and ph from an autonomous surface vehicle in a coastal upwelling system. *Deep Sea*
285 *Research Part II: Topical Studies in Oceanography*, 151, 137–146.
- 286 Chevallier, F.: On the parallelization of atmospheric inversions of CO₂ surface fluxes within a
287 variational framework, *Geosci. Model Dev.*, 6, 783–790, <https://doi.org/10.5194/gmd-6-783-2013>,
288 2013.
- 289 Chevallier, F., Fisher, M., Peylin, P., Serrar, S., Bousquet, P., Bréon, F.-M., Chédin, A., and Ciais, P.:
290 Inferring CO₂ 15 sources and sinks from satellite observations: Method and application to TOVS
291 data, *J. Geophys. Res. Atmos.*, 110, <https://doi.org/https://doi.org/10.1029/2005JD006390>, 2005.
- 292 Chevallier, F., Ciais, P., Conway, T. J., Aalto, T., Anderson, B. E., Bousquet, P., Brunke, E. G.,
293 Ciattaglia, L., Esaki, Y., Fröhlich, M., Gomez, A., Gomez-Pelaez, A. J., Haszpra, L., Krummel, P. B.,
294 Langenfelds, R. L., Leuenberger, M., Machida, T., Maignan, F., Matsueda, H., Morguí, J. A., Mukai,
295 H., Nakazawa, T., Peylin, P., Ramonet, M., Rivier, L., Sawa, Y., Schmidt, M., Steele, L. P., Vay, S. A.,
296 Vermeulen, A. T., Wofsy, S., and Worthy, D.: CO₂ surface fluxes at grid point scale estimated from
297 a global 21 year reanalysis of atmospheric measurements, *J. Geophys. Res. Atmos.*, 115,
298 <https://doi.org/https://doi.org/10.1029/2010JD013887>, 2010.
- 299 Droghei, R., Buongiorno Nardelli, B., and Santoleri, R.: A new global sea surface salinity and

density dataset from multivariate observations (1993–2016), *Frontiers in Marine Science*, 5, 84, 2018.

Feely, R. A., Takahashi, T., Wanninkhof, R., McPhaden, M. J., Cosca, C. E., Sutherland, S. C., and Carr, M.-E. Decadal variability of the air-sea CO₂ fluxes in the equatorial Pacific Ocean, *J. Geophys. Res.*, 111, C08S90, doi:10.1029/2005JC003129, 2006.

Feely, R. A., Sabine, C. L., Hernandez-Ayon, J. M., Ianson, D., & Hales, B. (2008). Evidence for upwelling of corrosive" acidified" water onto the continental shelf. *science*, 320 (5882), 1490–1492.

Friedlingstein, P., O'Sullivan, M., Jones, M. W., Andrew, R. M., Gregor, L., Hauck, J., Le Quéré, C., Luijkx, I. T., Olsen, A., Peters, G. P., Peters, W., Pongratz, J., Schwingshackl, C., Sitch, S., Canadell, J. G., Ciais, P., Jackson, R. B., Alin, S. R., Alkama, R., Arneeth, A., Arora, V. K., Bates, N. R., Becker, M., Bellouin, N., Bittig, H. C., Bopp, L., Chevallier, F., Chini, L. P., Cronin, M., Evans, W., Falk, S., Feely, R. A., Gasser, T., Gehlen, M., Gkritzalis, T., Gloege, L., Grassi, G., Gruber, N., Gürses, O., Harris, I., Hefner, M., Houghton, R. A., Hurtt, G. C., Iida, Y., Ilyina, T., Jain, A. K., Jersild, A., Kadono, K., Kato, E., Kennedy, D., Klein Goldewijk, K., Knauer, J., Korsbakken, J. I., Landschützer, P., Lefèvre, N., Lindsay, K., Liu, J., Liu, Z., Marland, G., Mayot, N., McGrath, M. J., Metzl, N., Monacchi, N. M., Munro, D. R., Nakaoka, S.-I., Niwa, Y., O'Brien, K., Ono, T., Palmer, P. I., Pan, N., Pierrot, D., Pocock, K., Poulter, B., Resplandy, L., Robertson, E., Rödenbeck, C., Rodriguez, C., Rosan, T. M., Schwinger, J., Séférian, R., Shutler, J. D., Skjelvan, I., Steinhoff, T., Sun, Q., Sutton, A. J., Sweeney, C., Takao, S., Tanhua, T., Tans, P. P., Tian, X., Tian, H., Tilbrook, B., Tsujino, H., Tubiello, F., van der Werf, G. R., Walker, A. P., Wanninkhof, R., Whitehead, C., Willstrand Wranne, A., Wright, R., Yuan, W., Yue, C., Yue, X., Zaehle, S., Zeng, J., and Zheng, B.: Global Carbon Budget 2022, *Earth System Science Data*, 14, 4811–4900, <https://doi.org/10.5194/essd-14-4811-2022>, 2022.

Garnesson, P., Mangin, A., Fanton d'Andon O., Demaria, J., Bretagnon, M., The CMEMS GlobColour chlorophyll-a product based on satellite observation: multi-sensor merging and flagging strategies, *Ocean Sci.*, 15, 819-830, Volume 15, issue 3, <https://doi.org/10.5194/os-15-819-2019>, 2019.

Good, S., Fiedler, E., Mao, C., Martin, M. J., Maycock, A., Reid, R., Roberts-Jones, J., Searle, T., Waters, J., While, J., and Worsfold, M.: The Current Configuration of the OSTIA System for Operational Production of Foundation Sea Surface Temperature and Ice Concentration Analyses, *Remote Sensing*, 12, <https://www.mdpi.com/2072-4292/12/4/720>, 2020.

Hersbach, H., Bell, B., Berrisford, P., Hirahara, S., Horányi, A., Muñoz-Sabater, J., Nicolas, J., Peubey, C., Radu, R., Schepers, D., Simmons, A., Soci, C., Abdalla, S., Abellan, X., Balsamo, G., Bechtold, P., Biavati, G., Bidlot, J., Bonavita, M., De Chiara, G., Dahlgren, P., Dee, D., Diamantakis, M., Dragani, R., Flemming, J., Forbes, R., Fuentes, M., Geer, A., Haimberger, L., Healy, S., Hogan, R. J., Hólm, E., Janisková, M., Keeley, S., Laloyaux, P., Lopez, P., Lupu, C., Radnoti, G., de Rosnay, P., Rozum, I., Vamborg, F., Villaume, S., and Thépaut, J.-N.: The ERA5 global reanalysis, *Q. J. Roy. Meteor. Soc.*, 146, 19992049, <https://doi.org/10.1002/qj.3803>, 2020.

Ho, D. T., Law, C. S., Smith, M. J., Schlosser, P., Harvey, M., & Hill, P. (2006). Measurements of air-sea gas exchange at high wind speeds in the Southern Ocean: Implications for global parameterizations. *Geophysical Research Letters*, 33 (16). Retrieved 2019-06-25, from <https://agupubs.onlinelibrary.wiley.com/doi/abs/10.1029/2006GL026817>, doi: 10.1029/2006GL026817.

343 Körtzinger, A.: Determination of carbon dioxide partial pressure ($p\text{CO}_2$), edited by: Grasshoff, K.,
 344 Kremling, K., and Ehrhardt, M., chap. 9, 149–158, John Wiley & Sons, Ltd,
 345 <https://doi.org/10.1002/9783527613984.ch9>, 1999.

346 Menemenlis, D., Campin, J., Heimbach, P., Hill, C., Lee, T., Nguyen, A., Schodlok, M., and Zhang,
 347 H.: ECCO2: High Resolution Global Ocean and Sea Ice Data Synthesis, 2008, OS31C-1292, 2008.

348 Naegler, T.: Reconciliation of excess ^{14}C -constrained global CO_2 piston velocity estimates, *Tellus*
 349 *B*, 61, 372–384, 2009.

350 Pujol, M., Schaeffer, P., Faugère, Y., Raynal, M., Dibarboure, G., and Picot, N.: Gauging the
 351 Improvement of Recent Mean Sea Surface Models: A New Approach for Identifying and
 352 Quantifying Their Errors, *J. Geophys. Res. Oceans*, 123, 5889–5911,
 353 <https://doi.org/10.1029/2017JC013503>, 2018.

354 Pujol, M.-I., Faugère, Y., Taburet, G., Dupuy, S., Pelloquin, C., Ablain, M., and Picot, N.: DUACS
 355 DT2014: the new multi-mission altimeter data set reprocessed over 20years, *Ocean Sci.*, 12,
 356 1067–1090, <https://doi.org/10.5194/os-12-1067-2016>, 2016.

357 Regnier, P., Resplandy, L., Najjar, R. G., & Ciais, P. (2022). The land-to-ocean loops of the global
 358 carbon cycle. *Nature*, 603 (7901), 401–410.
 359

360 Rödenbeck, C., Bakker, D. C. E., Gruber, N., Iida, Y., Jacobson, A. R., Jones, S., Landschützer, P.,
 361 Metzl, N., Nakaoka, S., Olsen, A., Park, G.-H., Peylin, P., Rodgers, K. B., Sasse, T. P., Schuster, U.,
 362 Shutler, J. D., Valsala, V., Wanninkhof, R., and Zeng, J.: Data-based estimates of the ocean carbon
 363 sink variability – first results of the Surface Ocean $p\text{CO}_2$ Mapping intercomparison (SOCOM),
 364 *Biogeosciences*, 12, 72517278, <https://doi.org/10.5194/bg-12-7251-2015>, 2015.
 365

366 Takahashi, T., Sutherland, S. C., Wanninkhof, R., Sweeney, C., Feely, R. A., Chipman, D. W., Hales,
 367 B., Friederich, G., Chavez, F., Sabine, C., Watson, A., Bakker, D. C., Schuster, U., Metzl, N.,
 368 Yoshikawa-Inoue, H., Ishii, M., Midorikawa, T., Nojiri, Y., Körtzinger, A., Steinhoff, T., Hoppema,
 369 M., Olafsson, J., Arnarson, T. S., Tilbrook, B., Johannessen, T., Olsen, A., Bellerby, R., Wong, C.,
 370 Delille, B., Bates, N., and de Baar, H. J.: Climatological mean and decadal change in surface ocean
 371 $p\text{CO}_2$, and net sea-air CO_2 flux over the global oceans, *Deep-Sea Res. Pt. 2*, 56, 554–577,
 372 <https://doi.org/10.1016/j.dsr2.2008.12.009>, 2009.
 373

374 Wang, X., Murtugudde, R., Hackert, E., Wang, J., and Beauchamp, J.: Seasonal to decadal
 375 variations of sea surface $p\text{CO}_2$ and sea-air CO_2 flux in the equatorial oceans over 1984–2013: A
 376 basin-scale comparison of the Pacific and Atlantic Oceans, *Global Biogeochem. Cy.*, 29, 597–609,
 377 <https://doi.org/10.1002/2014GB005031>, 2015.
 378

379 Wanninkhof, R.: Relationship between wind speed and gas exchange over the ocean revisited,
 380 *Limnol. Oceanogr.-Meth.*, 12, 351–362, <https://doi.org/10.4319/lom.2014.12.351>, 2014.

381 Weiss, R.: Carbon dioxide in water and seawater: the solubility of a non-ideal gas, *Mar. Chem.*, 2,
 382 203–215, [https://doi.org/10.1016/0304-4203\(74\)90015-2](https://doi.org/10.1016/0304-4203(74)90015-2), 1974.

383 Zhang, Y., Xu, H., Qiao, F. *et al.* Seasonal variation of the global mixed layer depth: comparison
 384 between Argo data and FIO-ESM. *Front. Earth Sci.* 12, 24–36 (2018).
 385 <https://doi.org/10.1007/s11707-017-0631-6>